Journal of Materials Chemistry A

Accepted Manuscript

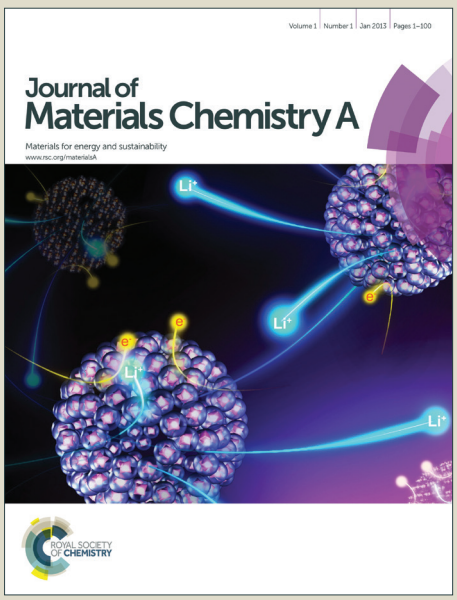

ROYAL SOCIETY OF CHEMISTRY

www.rsc.org/materialsA

Journal Name

RSCPublishing

ARTICLE

Photocatalytic water oxidation under visible light by valence band controlled oxynitride solid solutions $LaTaON_2$–$SrTiO_3$

Cite this: DOI: 10.1039/x0xx00000x

Received 00th January 2012,
Accepted 00th January 2012

DOI: 10.1039/x0xx00000x

www.rsc.org/

Hideki Kato,*[a] Koichiro Ueda,[†a] Makoto Kobayashi,[a] Masato Kakihana[a]

The solid solutions between $LaTaON_2$ and $SrTiO_3$ were successfully synthesized. In this solid solution, the valence band maxima (VBM) shifted to positive sides as the fraction of $SrTiO_3$ increased, resulting in the appearance of activity for O_2 evolution even without any cocatalysts. Despite of widening of the band gap (E_g) by only 0.15 eV, $La_{0.5}Sr_{0.5}Ta_{0.5}Ti_{0.5}O_2N$ gained 0.5 V larger driving force for water oxidation, which corresponds to potential difference between VBM and potential for water oxidation, than $LaTaON_2$. It suggested that the contribution of Ti 3d to the conduction band suppressed the widening of E_g. This is an interesting feature in the present $LaTaON_2$–$SrTiO_3$ solid solution. The bare $La_{0.5}Sr_{0.5}Ta_{0.5}Ti_{0.5}O_2N$ exhibited the activity for O_2 evolution 9 times higher than $LaTaON_2$ modified with a CoO_x cocatalyst. It has been found that the driving force for water oxidation of $La_{0.5}Sr_{0.5}Ta_{0.5}Ti_{0.5}O_2N$ was 0.8 V, and was larger than those in other perovskite-type oxynitrides.

1. Introduction

Photocatalytic water splitting is a potential candidate for solar hydrogen production.[1–4] To date, some photocatalysts including Z-scheme systems have achieved overall water splitting under visible light.[5–16] Their efficiencies are not high enough to push photocatalytic water splitting in practical use at this time. Construction of highly active photocatalysts is necessary to realize solar fuel production by photocatalysis. Therefore, developments of new methodology to improve photocatalytic performance and new photocatalyst materials are still important subjects. Oxidation of water to O_2 is a fundamental reaction in overall water splitting besides reduction of protons to H_2. We have demonstrated the achievement of water oxidation without assistance of cocatalysts through control of valence band potentials in $LaTaON_2$–$NaTaO_3$ oxynitride solid solutions[17] despite of no activity in the native $LaTaON_2$.[18] Where VBM becomes more positive than that in the native $LaTaON_2$ according to the decreases in contents of nitrogen. Takata *et al.* have recently achieved overall water splitting by the $LaTaON_2$–$LaMg_{2/3}Ta_{1/3}O_3$ solid solution photocatalysts which function under visible light up to 600 nm of wavelength.[16] In the $LaTaON_2$–$LaMg_{2/3}Ta_{1/3}O_3$ photocatalysts, coating of SiO_2 and/or TiO_2 layer on $(Rh,Cr)_2O_3$ cocatalyst-loaded photocatalyst plays an important role in inhibition of reduction of O_2 to achieve steady water splitting. However, water splitting does not take place over $LaTaON_2$ even with the coating modification because the native $LaTaON_2$ lacks the ability for water oxidation. Giving the ability for water oxidation through the formation of solid solutions is also indispensable to achieve water splitting using the $LaTaON_2$–$LaMg_{2/3}Ta_{1/3}O_3$ photocatalysts. Thus, the control of band potentials is very important methodology to fabricate photocatalysts.

As mentioned above, we have previously succeeded in giving the $LaTaON_2$–$NaTaO_3$ solid solution the ability for water oxidation. However, the band gaps (E_g) of the solid solutions become wide as the nitrogen contents decrease. This means narrowing the range of wavelengths available, and is a drawback in the $LaTaON_2$–$NaTaO_3$ solid solution. Such widening of E_g would be suppressed when both conduction and valence bands potentials shifts toward positive sides. In this sense, $SrTiO_3$ with a perovskite structure can be regard as a candidate for the end member in the band potential controlled solid solution based on $LaTaON_2$ because contribution of Ti 3d to the conduction band may shift the conduction band minimum (CBM) positively.

In this work, we synthesized a new series of $LaTaON_2$-based solid solution, $LaTaON_2$–$SrTiO_3$, with the aim of development of new visible-light-driven photocatalysts possessing abilities for reduction and oxidation of water. The effects of incorporation of Ti on the band potentials and photocatalytic properties are also discussed.

2. Experimental section

2.1 Synthesis of $LaTaON_2$–$SrTiO_3$ solid solution

Powders of $LaTaON_2$–$SrTiO_3$ solid solutions were obtained by nitridation of oxide precursors prepared by a polymerizable complex method employing citric acid (Wako Pure Chemical, 98%) and propylene glycol (Kanto Chemical, 99.0%) as described elsewhere.[17] Strontium carbonate (Kanto Chemical, 99.9%), titanium tetrabutoxide (Kanto Chemical, 97.0%), lanthanum nitrate hexahydrate (Wako Pure Chemical, 99.9%)

and tantalum chloride (Furuuchi, 99.9%) were used as raw materials. Nitridation of 1.0 g of oxide precursors was performed under an NH_3 stream (100 mL min^{-1}) at 1273 K for 15 h using a tubular furnace made of alumina. The samples with different compositions according to the formula $La_{1-x}Sr_xTa_{1-x}Ti_xO_{1+2x}N_{2-2x}$ were synthesized. These samples are described simply as Sr100*x* in this paper.

2.2 Characterization of samples

The samples obtained were characterized by X-ray diffraction (XRD; Bruker AXS, D2 Phaser), ultraviolet-visible spectroscopy in a diffuse reflectance method (UV-vis; Shimadzu, UV-3100), nitrogen content analysis (Horiba, EMGA-620W) and nitrogen adsorption analysis (Micromeritics, ASAP 2010) with the similar manner reported in the literature.[17] Photoelectrochemical analysis of the samples was performed using photocatalyst-deposited fluorine-doped tin oxide (FTO) substrates. Photocatalyst particles were deposited on FTO by an electrophoretic method (10 V for 60 s) in 40 mL of acetone containing 30 mg of the sample and 10 mg of I_2.[19] Current–potential curves were taken by linear sweep voltammetry with a sweep rate –10 mV s^{-1} in an aqueous 0.1 M K_2SO_4 solution at pH 4.2–11.1 under intermitted visible light. NaOH and H_2SO_4 were used to adjust pH values of the electrolyte solution. Platinum and Ag/AgCl electrodes were used as counter and reference electrodes, respectively.

2.3 Evaluation of photocatalytic properties

Photocatalytic activities of the oxynitride solid solutions for H_2 or O_2 evolution in the presence of a sacrificial reagent were evaluated using a gas-closed circulation system. The samples modified with 0.3 wt% of Pt cocatalyst were used for H_2 evolution. The Pt cocatalyst was deposited by an impregnation method with sequent reduction treatment under a H_2 flow (30 mL min^{-1}) at 473 K for 1 h. For O_2 evolution, the bare samples were used in typical experiments although modification by a CoO_x cocatalyst (1 wt% as metal) was also examined for $LaTaON_2$ and Sr50.[20] The CoO_x cocatalyst was deposited by an impregnation method using an aqueous $Co(NO_3)_2$ solution followed by calcination under an NH_3 flow at 773 K for 1 h.[21] 0.1 g of photocatalyst was dispersed in a reactant solution (150 mL), 10 vol% methanol for H_2 evolution while 20 mM $AgNO_3$ containing 0.1 g of La_2O_3 for O_2 evolution. After deaeration of the system, 10 kPa of Ar was introduced into the system. The suspended solution was irradiated with visible light (λ > 420 nm) using a 300-W Xe arc lamp (Excelitas, Cermax PE300BF) with an optical cut-off filter. Monochromatic light at 460 nm extracted by an interference band-pass filter was used for determination of an apparent quantum yield. Gaseous products were analysed using an online gas chromatograph (Shimadzu, GC-8A; MS-5A column; TCD detector; Ar carrier).

3. Results and discussion

3.1 Synthesis and characterization of solid solutions

Oxide precursors were obtained as white amorphous powder. Nitridation of the precursor at 1273 K for 15 h gave a perovskite-type compound without impurities for all compositions as shown in Fig. 1A. This is different from the synthesis of the previous $LaTaON_2$-$NaTaO_3$ solid solution, which requires adjustment of nitriding time to obtain a single phase of the sample according to the compositions because of volatilization of Na.[17] The absence of highly volatile elements such as alkaline metals caused easiness in the synthesis of the present $LaTaON_2$–$SrTiO_3$ solid solution. This point should be noticed as one superior feature in the $LaTaON_2$–$SrTiO_3$ system to $LaTaON_2$–$NaTaO_3$. Diffraction peaks shifted toward higher angles with increasing the fraction of $SrTiO_3$. Analysis of lattice parameters from the XRD patterns revealed that cell volumes changed linearly along with the compositions obeying to the Vegard's law (Fig. 1B). Control of the content of nitrogen is a key factor in tuning of VBM in this solid solution. The elemental analysis revealed that the contents of nitrogen decreased with increasing the fraction of $SrTiO_3$ although small deviations from the ideal values were seen (Table 1). Thus, it was confirmed that the control of the contents of nitrogen was achieved by the formation of $LaTaON_2$–$SrTiO_3$ solid solutions as well as the previous $LaTaON_2$–$NaTaO_3$ system. The specific surface area (S_{BET}) of the solid solution was remarkably decreased from 16.5 to 9.9 m^2 g^{-1} at the first step of the solid solution (Sr25). The solid solutions with further substitution tended to decrease in S_{BET} however the changes in S_{BET} were not remarkable (Table 1).

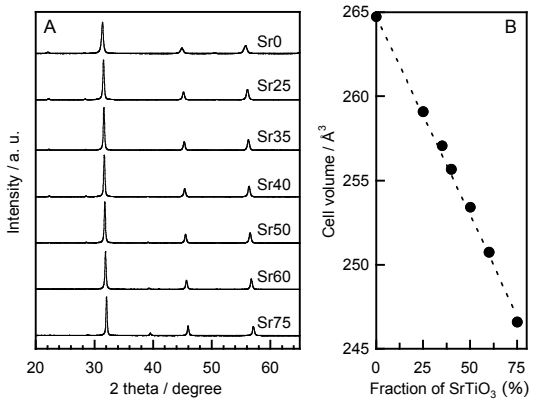

Fig. 1 (A) XRD patterns and (B) cell volumes of $LaTaON_2$–$SrTiO_3$.

Table 1 Properties of $LaTaON_2$–$SrTiO_3$ solid solutions

Sample	Content of N (wt%)		S_{BET} (m^2 g^{-1})	E_g (eV)
	measured	ideal		
Sr0	7.93	7.70	16.5	2.04
Sr25	6.88	6.59	9.9	2.12
Sr35	6.25	6.05	9.1	2.13
Sr40	6.10	5.76	8.4	2.16
Sr50	5.22	5.12	7.9	2.19
Sr60	4.34	4.38	8.4	2.21
Sr75	2.97	3.06	7.6	2.28

Fig. 2 shows normalized UV-vis spectra of the $LaTaON_2$–$SrTiO_3$ solid solutions. The samples except for $LaTaON_2$ (Sr0) exhibited background absorption in addition to the band gap absorption. The origin of the background absorption would be the reduced metal ions, Ti^{3+} and/or Ta^{4+} in the present case, which are formed during the nitriding process.[10] The absorption attributed to the band gap excitation shifted to high-energy (shorter wavelength) sides with increasing the fraction of $SrTiO_3$. The band gaps (E_g) estimated from the onsets on the

background absorption are listed in Table 1. In the $LaTaON_2$–$NaTaO_3$, E_g was 2.23, 2.38 and 2.76 for Na25, Na50 and Na75, respectively.[17] The E_g of $LaTaON_2$–$SrTiO_3$ was narrower than that in $LaTaON_2$–$NaTaO_3$ when compared at the same fraction of oxide. Thus, it was confirmed that widening of E_g accompanying the substitution was remarkably suppressed in the present $LaTaON_2$–$SrTiO_3$ system. The plausible explanation of the differences in E_g between these two systems is the positive shift of CBM due to the contribution of Ti 3d.

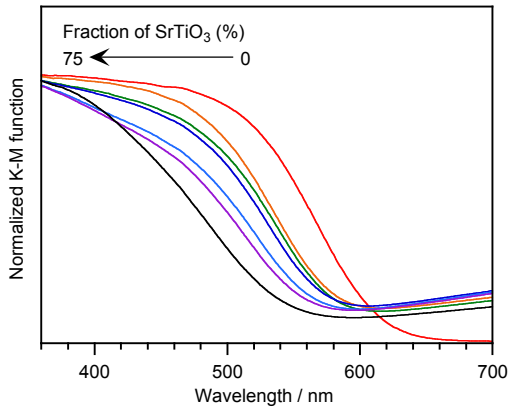

Fig. 2 UV-vis spectra of $LaTaON_2$–$SrTiO_3$.

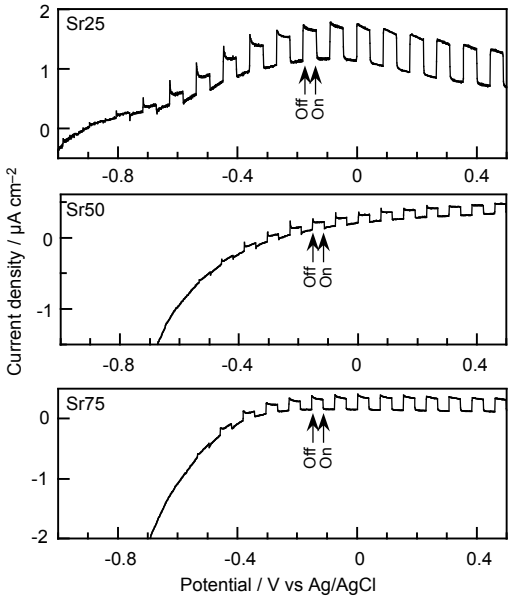

Fig. 3 Current-potential curves of $LaTaON_2$–$SrTiO_3$ taken under intermitted visible light irradiation. Electrolyte solution: 0.1 M K_2SO_4 at pH6.4.

Photoelectrochemical analysis was conducted for Sr25, Sr50 and Sr75 to obtain information about band potentials. Current–potential curves taken under intermitted visible light irradiation in a 0.1 M aqueous K_2SO_4 solution at pH 6.4 are presented in Fig. 3. All samples exhibited anodic photoresponse, indicating that these three samples had negative-type semiconducting nature. In this work, the potential where the photoresponse disappears was regarded as the flat band potential (E_{fb}). The E_{fb} shifted to positive side as the fraction of $SrTiO_3$ increased. The band potentials estimated from E_{fb} and E_g are depicted in Fig. 4A. Where the potentials of CBM are assumed to be 0.2 V above E_{fb}, and the potentials of $LaTaON_2$ are illustrated referring the previous report.[17] The CBM of $LaTaON_2$–$SrTiO_3$ shifted to lower (more positive) positions with increasing the fraction of $SrTiO_3$ although that shifted negatively in the $LaTaON_2$–$NaTaO_3$ system. Contribution of Ti 3d to the formation of CB would be a predominant factor for the positive shifts of CBM observed in the $LaTaON_2$–$SrTiO_3$ as expected. The VBM of the $LaTaON_2$–$SrTiO_3$ solid solution shifted to lower positions monotonically; 1.10, 1.45 and 1.54 V vs E(Ag/AgCl) for Sr25, Sr50 and Sr75, respectively. In the case of $LaTaON_2$–$NaTaO_3$, the positions of VBM are 1.13, 1.08 and 1.12 V for Na25, Na50 and Na75, respectively.[17] It should be noticed that the present solid solutions allow tuning of the VBM potential in wider range than the $LaTaON_2$–$NaTaO_3$ solid solutions. The relatively large shift in VBM with small widening of E_g is an interesting feature of the $LaTaON_2$–$NaTaO_3$ system. For example, in Sr50, 0.5 V of positive shift in the VBM is achieved with widening of E_g by only 0.15 eV. The photoelectrochemical measurements at pH 4.2–11.1 revealed that band positions in Sr50 shifted parallel to $E(H^+/H_2)$ and $E(O_2/H_2O)$ as reported for other oxynitrides (Figs. S1 and 4B).[22–24]‡

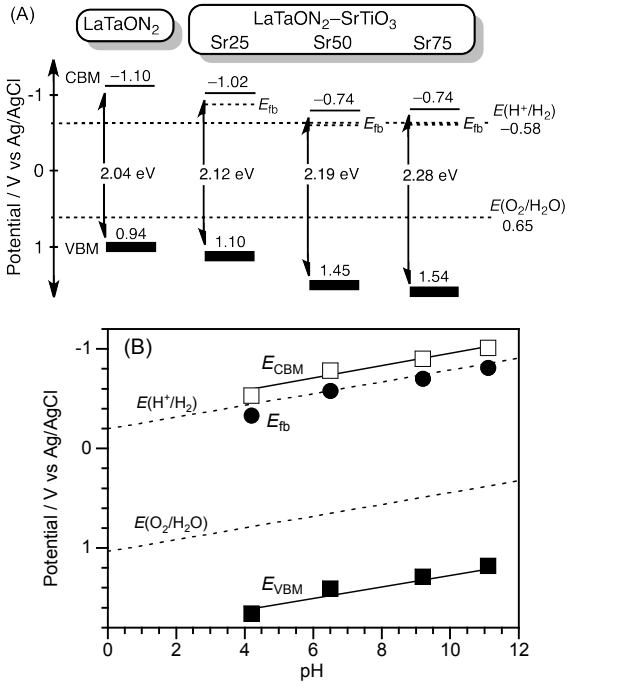

Fig. 4 (A) Estimated band potentials for $LaTaON_2$–$SrTiO_3$ at pH 6.4 and (B) changes in band potentials of $La_{0.5}Sr_{0.5}Ta_{0.5}Ta_{0.5}O_2N$ with different pH values.

3.2 Photocatalytic properties

Photocatalytic activities of the solid solutions for H_2 or O_2 from water containing a sacrificial electron donor (methanol) or acceptor (Ag^+ ion) under visible light (λ > 420 nm) are summarized in Fig. 5. All Pt(0.3 wt%)-loaded samples

produced H_2 whereas the activity for H_2 evolution gradually decreased along with the $SrTiO_3$ substitution. It is basically due to the positive shifts in CBM corresponding to the decrease in the driving force for reduction of water. All $SrTiO_3$-substituted samples produced O_2 even in the absence of cocatalysts while the native $LaTaON_2$ was inactive. The appearance of ability for O_2 evolution is caused by obtaining the driving force for water oxidation, corresponding to the potential difference (ΔE) between VBM and potential for water oxidation ($E(O_2/H_2O)$, enough to proceed the reaction. We have previously reported that ΔE larger than 0.4 V is required for perovskite-type oxynitrides to oxidize water without the assistance of cocatalysts.[17] The appearance of ability for O_2 evolution in Sr25 also meets this account since ΔE assumed in Sr25 is 0.45 V as shown in Fig. 4. The O_2 evolution was enhanced with increasing the fraction of $SrTiO_3$ while the activity decreased beyond Sr50. The appearance of background absorption in the UV-vis spectra implies the contribution of band bending, which facilitates migration of holes to surface, to enhancement of O_2 evolution.[25] However, such a band bending effect is limited in the present solid solution system because there are no remarkable differences in intensity of the background absorption between samples except for $LaTaON_2$. Therefore, the enhancement of the activity for O_2 evolution beyond Sr25 is resulted by the increase in the driving force. The O_2 evolution rate in Sr75 (42 μmol h^{-1}) was 40% of that in Sr50 (104 μmol h^{-1}). This is not explained from the band potentials because Sr75 has a larger ΔE than Sr50. The decrease in the number of available photons caused by widening of E_g may participate decreasing the activity. However, this effect seems to be not predominant because of the small difference in E_g between Sr50 and Sr75 as shown in Fig. 2. For H_2 evolution, Sr75 also exhibited the half activity of Sr50 although their driving force for H_2 production was almost the same. These results suggest that the remarkable decreases in the activity of Sr75 for both H_2 and O_2 evolution in comparison with Sr50 are attributed to other reasons. It is one possible explanation that Sr75 has defects, which facilitate recombination of photogenerated electrons and holes, more than Sr50. Another possibility is low mobility of holes in the VB of Sr75 due to the small contribution of nitrogen to the VB. The highest rate for O_2 evolution was obtained by Sr50, and was higher than the rates reported for $La_{0.75}Na_{0.25}TaO_{1.5}N_{1.5}$ (4.9 μmol h^{-1}) and $LaTiO_2N$ (25 μmol h^{-1}) in the absence of cocatalysts.[17,26] The driving force for water oxidation in Sr50 (0.80 V) is larger than those in $La_{0.75}Na_{0.25}TaO_{1.5}N_{1.5}$ (0.48 V) and $LaTiO_2N$ (*ca.* 0.6 V).[17,23] It is reasonably accepted that the largest driving force of Sr50 brings the highest activity in the absence of cocatalysts. The apparent quantum yield of Sr50 was determined to be 2.2% using monochromatic light at 460 nm with 225 mW of incident power. Fig 6 shows reaction time courses of O_2 evolution using Sr50. Sr50 produced O_2 in a high rate at the early stage of the reaction, however the rate was remarkably suppressed, especially after 1 h. Shielding photons and blocking active sites by metallic Ag particles photodeposited on the surface were considered as reasons for the decrease in the rate of O_2 evolution as usually explained in the O_2 evolution using Ag^+ ions as the electron acceptor. The sample used for 5 h of reaction was the mixture of Ag-deposited Sr50 and $La(OH)_3$ used for buffering pH. The Ag and $La(OH)_3$ were washed out by *ca.* 3 mL of concentrated HNO_3 under the suction filtration condition. Then, O_2 evolution was examined using the after reaction sample to check the durability of Sr50. The after reaction sample produced O_2 with a high rate in the early stage again. Where, its activity was recovered in 60% of that for the fresh sample. In addition, the amount of N_2, which was produced by self-oxidation of unstable N^{3-} by holes, was significantly reduced in the second use as observed for other oxynitride photocatalysts.[27] To check the damage by the HNO_3-treatment, the fresh Sr50 was also treated with concentrated HNO_3 like as the after reaction sample. The activity of the HNO_3-treated sample was 71% of that obtained for the fresh sample. These results indicated that the predominant reason for the deactivation during the reaction was due not to the collapse of the sample but to the deposition of Ag particles on the surface. Thus, it was proven that Sr50 had the moderate stability against photocatalysis.

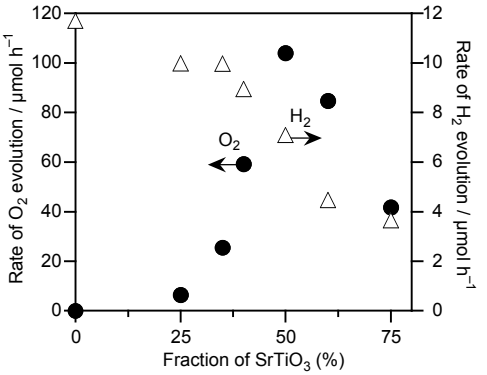

Fig. 5 Photocatalytic activities of $LaTaON_2$–$SrTiO_3$ for H_2 and O_2 evolution under visible light (λ > 420 nm). For H_2 evolution: Pt(0.3 wt%) cocatalyst, 10 vol% methanol. For O_2 evolution: no cocatalyst, 20 mM $AgNO_3$, 0.1 g of La_2O_3.

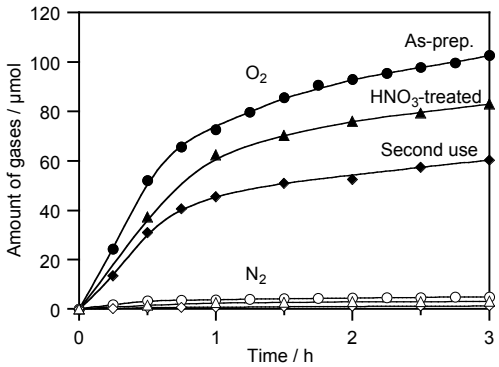

Fig. 6 Reaction time course for O_2 evolution under visible light using $La_{0.5}Sr_{0.5}Ta_{0.5}Ta_{0.5}O_2N$; as-prepared, the second use after washing with HNO_3 and HNO_3-treated. Catalyst: 0.1 g, 20 mM $AgNO_3$, 0.1 g of La_2O_3.

As described above, the fabrication of visible-light-driven photocatalysts capable of both H_2 and O_2 evolution in the presence of sacrificial reagents has been achieved by the

formation of $LaTaON_2$–$SrTiO_3$ solid solution. In Sr35–75, the rates of H_2 evolution were much lower than those of O_2 evolution. This implies the presence of electron traps where the electrons lose their potential. Accordingly, some electrons trapped are not capable of reducing of H^+ whereas they are still able to reduce Ag^+.

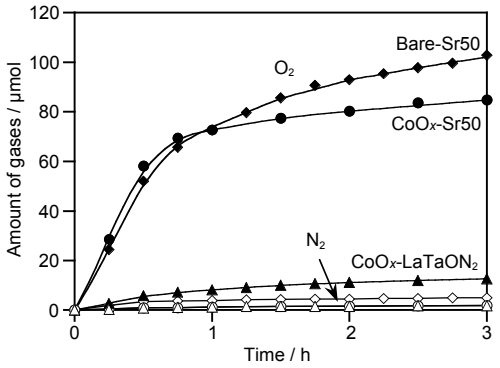

Fig. 7 O_2 evolution over bare and CoO_x-loaded Sr50 and CoO_x-loaded $LaTaON_2$. Catalyst: 0.1 g, 20 mM $AgNO_3$, 0.1 g of La_2O_3.

3.3 The effects of CoO_x cocatalysts

The effects of the CoO_x cocatalyst on the O_2 evolution were examined for $LaTaON_2$ and Sr50 (Fig. 7). $LaTaON_2$ modified with CoO_x (1 wt% as metal) produced O_2 although the bare sample was inactive as mentioned above. Thus, it is confirmed that O_2 evolution by $LaTaON_2$ can be achieved not only by tuning of VBM but also by modification with cocatalysts. However, it should be noticed that the activity of CoO_x-loaded $LaTaON_2$ (11.7 μmol h^{-1}) was much less than that of bare Sr50 (104 μmol h^{-1}). The CoO_x cocatalyst also enhanced the O_2 evolution over Sr50 besides the suppression of N_2 formation, however the enhancement was not significant. An important role of the CoO_x cocatalyst is the function as active sites driving water oxidation with small overpotentials.[20,28] The CoO_x cocatalyst is effective for photocatalysts and photoanodes especially ones possessing small driving forces such as $LaTiO_2N$, $BaTaO_2N$ and $LaTaON_2$.[24,26] In the case of Sr50, the low rate of the hole supply to the reaction sites due to the recombination in the bulk would limit the boost in the O_2 evolution by the CoO_x cocatalyst, implying the further improvement of performance by preparation of the high quality samples.

4. Conclusion

The $LaTaON_2$–$SrTiO_3$ solid solutions have superior features, easiness in the synthesis, suppression of widening of E_g and large driving force for water oxidation, in comparison with the $LaTaON_2$–$NaTaO_3$ solid solutions reported previously. In addition, it has been found that tuning of band potentials through the formation of the $LaTaON_2$–$SrTiO_3$ solid solutions is more effective methodology to obtain the activity for the O_2 evolution using the $LaTaON_2$-based photocatalysts than the modification with the CoO_x cocatalyst. Thus, this work has revealed that the $LaTaON_2$–$SrTiO_3$ solid solutions are potential candidates for photocatalysts and photoanodes with the aim of overall water splitting under visible light.

Acknowledgements

This work was supported by a Grain-in-Aid (No. 24107004) for Innovative Areas "Photosynthesis" (Area No. 2406) from MEXT, Japan.

Notes and references

[a] Institute of Multidisciplinary Research for Advanced Materials, Tohoku University, 2-1-1 Katahira, Aoba-ku, Sendai 980-8577, Japan

† Electronic Supplementary Information (ESI) available: Current-potentials curves for Sr50 at pH4.2–11.1. See DOI: 10.1039/b000000x/.

‡ Present address: Department of Chemical Engineering, School of Engineering, The University of Tokyo, 7-3-1 Hongo, Bunkyo-ku, Tokyo 113-8656, Japan

1. F. E. Oserloh, *Chem. Mater.*, 2008, **20**, 35.
2. A. Kudo and Y. Miseki, *Chem. Soc. Rev.*, 2009, **38**, 253.
3. X. Chen, S. Shen, L. Guo and S. Mao, *Chem. Rev.*, 2010, **110**, 6503.
4. B. A. Pinaud, J. D. Benck, L. C. Seitz, A. J. Forman, Z. Chen, T. G. Deutsch, B. D. James, K. N. Baum, G. N. Baum, S. Ardo, H. Wang, E. Miller and T. F. Jaramillo, *Energy Environ. Sci.*, 2013, **6**, 1983.
5. K. Sayama, K. Mukasa, R. Abe, Y. Abe and H. Arakawa, *J. Photochem. Photobiol. A*, 2002, **148**, 71.
6. R. Abe, T. Takata, H. Sugihara and K. Domen, *Chem. Commun.*, 2005, 3829.
7 K. Maeda, K. Teramura, D. Lu, T. Takata, N. Saito, Y. Inoue and K. Domen, *Nature*, 2006, **440**, 295.
8 Y. Lee, K. Teramura, M. Hara and K. Domen, *Chem. Mater.*, 2007, **19**, 2120.
9 H. Liu, J. Yuan, W. Shangguan and Y. Teraoka, *J. Phys. Chem. C*, 2008, **112**, 8521.
10 M. Higashi, R. Abe, T. Takata and K. Domen, *Chem. Mater.*, 2009, **21**, 1543.
11 Y. Sasaki, H. Nemoto, K. Saito and A. Kudo, *J. Phys. Chem. C*, 2009, **113**, 17536.
12 Y. Sasaki, H. Kato and A. Kudo, *J. Am. Chem. Soc.*, 2013, **135**, 5441.
13 H. Kato, Y. Sasaki, N. Shirakura and A. Kudo, *J. Mater. Chem. A*, 2013, **1**, 12327.
14 R. Asai, H. Nemoto, Q. JIa, K. Saito, A. Iwase and A. Kudo, *Chem. Commun.*, 2014, **50**, 2543.
15 K. Iwashina, A. Iwase, Y. H. Ng, R. Amal and A. Kudo, *J. Am. Chem. Soc.*, 2015, **137**, 604.
16 C. Pan, T. Takata, M. Nakabayashi, T. Matsumoto, N. Shibata, Y. Ikuhara and K. Domen, *Angew. Chem. Int. Ed.*, 2015, **54**, 295.
17 K. Ueda, H. Kato, M. Kobayashi, M. Hara and M. Kakihana, *J. Mater. Chem. A*, 2013, **1**, 3667.
18 M. Liu, W. You, Z. Lei, T. Takata, K. Domen and C. Li, *Chin. J. Catal.*, 2006, **27**, 556.
19 Y. Matsumoto, A Funatsu, D. Matsuo, U. Unal, *J. Phys. Chem. B*, 2001, **105**, 10893.
20 F. Jiao and H. Frei, *Angew. Chem. Int. Ed.*, 2009, **48**, 1841.
21 S. S. K. Ma, T. Hisatomi, K. Maeda, Y. Moriya and K. Domen, *J. Am. Chem. Soc.*, 2012, **134**, 19993.

22 W.-J. Chun, A. Ishikawa, H. Fujisawa, T. Takata, J. N. Kondo, M. Hara, M. Kawai, Y. Matsumoto and K. Domen, *J. Phys. Chem. B*, 2003, **107**, 1798.
23 C. L. Paven-Thivet, A. Ishikawa, A. Ziani, L. L. Gendre, M. Yoshida, J. Kubota, F. Tessier and K. Domen, *J. Phys. Chem. C*, 2009, **113**, 6156.
24 K. Maeda and K. Domen, *J. Catal.*, 2014, **310**, 67.
25 K. Maeda, D. Lu and K. Domen, *Angew. Chem. Int. Ed.*, 2013, **52**, 6488.
26 F. Zhang, A. Yamakata, K. Maeda, Y. Moriya, T. Takata, J. Kubota, K. teshima, S. Oishi and K. Domen, *J. Am. Chem. Soc.*, 2012, **134**, 8348.
27 G. Hitoki, T. Takata, J. N. Kondo, M. Hara, H. Kobayashi and K. Domen, *Chem. Commun.*, 2002, 1698.
28 J. Yang, D. Wang, H. Han and C. Li, *Accounts Chem. Res.*, 2013, **46**, 1900.

Table of contents entry

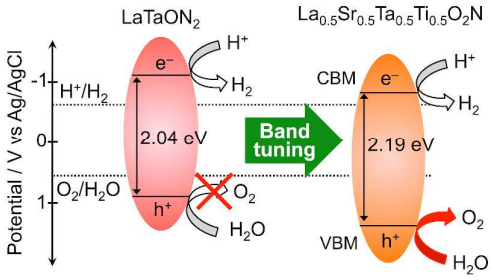

Visible-light-driven photocatalysts capable of both H_2 and O_2 evolution in the presence of sacrificial reagents have been developed through the formation of solid solutions between $LaTaON_2$ and $SrTiO_3$.